Inorganic Chemistry

Article

pubs.acs.org/IC

Coulombic Aggregations of Mn^{III} salen-Type Complexes and Keggin-Type Polyoxometalates: Isolation of Mn_2 Single-Molecule Magnets

Yuki Sawada, Wataru Kosaka, Yoshihito Hayashi, and Hitoshi Miyasaka*

Department of Chemistry, Division of Material Sciences, Graduate School of Natural Science and Technology, Kanazawa University, Kakuma-machi, Kanazawa, Ishikawa 920-1192, Japan

Supporting Information

ABSTRACT: The reaction of Mn^{III} salen-type complexes with di- and tetraanionic α-Keggin-type polyoxometalates (POMs) was performed, and three types of Coulombic aggregations containing Mn^{III} out-of-plane dimeric units (abbreviated as $[Mn_2]^{2+}$) that are potentially single-molecule magnets (SMMs) with an $S_T = 4$ ground state were synthesized: $[Mn_2(5\text{-MeOsaltmen})_2(acetone)_2][SW_{12}O_{40}]$ (**1**), $[Mn_2(salen)_2(H_2O)_2]_2[SiW_{12}O_{40}]$ (**2**), and $[Mn(5\text{-Brsaltmen})(H_2O)(acetone)]_2[\{Mn_2(5\text{-Brsaltmen})_2\}(SiW_{12}O_{40})]$ (**3**), where 5-Rsaltmen^{2-} = *N*,*N*′-(1,1,2,2-tetramethylethylene)bis(5-R-salicylideneiminate) with R = MeO (methoxy), Br (bromo) and salen^{2-} = *N*,*N*′-ethylenebis(salicylideneiminate). Compound **1** with a dianionic POM, $[SW_{12}O_{40}]^{2-}$, is composed of a 1:1 aggregating set of $[Mn_2]^{2+}$/POM, and **2**, with a tetraanionic POM, $[SiW_{12}O_{40}]^{4-}$, is a 2:1 set. Compound **3** with $[SiW_{12}O_{40}]^{4-}$ forms a unique 1D coordinating chain with a $[-\{Mn_2\}-POM-]^{2-}$ repeating unit, for which a hydrogen-bonded dimeric unit ($[Mn(5\text{-Brsaltmen})(H_2O)(acetone)]_2^{2+}$) is present as a countercation. Independent of the formula ratio of $[Mn_2]^{2+}$/POM, Mn^{III} dimers and POM units in **1**−**3** form respective segregated columns along a direction of the unit cell, which make an alternate packing to separate evenly identical species in a crystal. The nearest intermolecular Mn···Mn distance is found in the order **2** < **3** < **1**. The segregation of the $[Mn_2]^{2+}$ dimer resulted in interdimer distances long enough to effectively reduce the intermolecular magnetic interaction, in particular in **1** and **3**. Consequently, an intrinsic property, SMM behavior, of Mn^{III} dimers has been characterized in this system, even though the interdimer interactions are still crucial in the case of **2**, where a long-range magnetic order competitively affects slow relaxation of the magnetization at low ac frequencies.

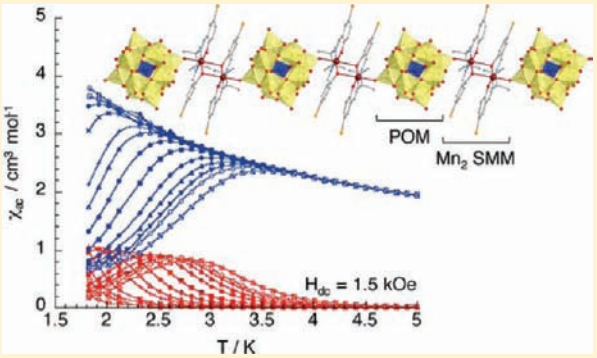

INTRODUCTION

Mn^{III} salen-type complexes (salen = *N*,*N*′-ethylenebis(salicylideneiminate)) act not only as a good coordinating-acceptor building module for molecular assemblies but also as a specific magnetic source that causes appropriate uniaxial anisotropy with a well-defined easy axis of the magnetization.[1] With the goal of designing magnetic assemblies, this type of complex has thus been assembled with paramagnetic coordinating-donor building units such as polycyanometalate as $[M(CN)_6]^{3-}$ to obtain various kinds of heterometallic magnetic materials having structural diversity from discrete molecules to three-dimensional (3D) frameworks.[1] The resulting magnets include superparamagnets[2] such as single-molecule magnets (SMMs)[3−7] and single-chain magnets (SCMs),[7b,8−12] where Mn^{III} salen-type complexes are efficiently utilized as uniaxial anisotropic sources by aligning their easy axes in one direction of the molecular topology.[12] In addition to controlling the magnetic anisotropy, another important point for the design of such SMMs and SCMs is to reduce magnetic interactions between respective low-dimensional entities of discrete units and chains, because long-range magnetic ordering owing to unignorable intermolecular or interchain interactions essentially excludes superparamagnetism.[13] This is in contrast to the synthetic strategy for classical magnets. For this purpose, the aggregation with bulky diamagnetic counterions is an efficient way to separate magnetic entities, and indeed, a few examples that were rationally designed along this strategy have been reported so far.[9d,14] The group of Li, Clérac, and Wang has used diamagnetic polyoxometalate (POM) clusters, $[XMo_6(OH)_6O_{18}]^{3-}$ (X = Al, Cr), as counterions for Mn^{III} salen dimers[15] and successfully extracted the SMM character of the Mn^{III} dimer, while the interdimer interactions for crystals of $[Mn^{III}(salen)(H_2O)]_2(ClO_4)_2$ itself have canceled out such an intrinsic character.[16] The combination of superparamagnetism with POMs was advanced in a unique molecular design, in which POMs were employed as "bulky ligands" to design isolated SMM or single-ion magnets (SIMs).[17−19] Thus, POMs act as an efficient spacer to magnetically isolate paramagnetic species, but meanwhile, they have diverse characteristics depending on the POMs used such as (i) discrete but 3D polyhedral clusters with different shape and size, (ii) relatively

Received: January 29, 2012
Published: April 2, 2012

dx.doi.org/10.1021/ic300215q | *Inorg. Chem.* 2012, 51, 4824−4832

high valence states, (iii) the coordination affinity of terminal oxygen atoms, (iv) redox activity, (v) the magnetic nature, (vi) pH stability, (vii) reaction and catalytic activities with various kinds of substrates, and so on.[20−22] These characteristics of POMs should be important factors to decide structural/packing motives and the nature of aggregations. Therefore, such diversities of characteristics in POMs motivated us to investigate the aggregations of POMs with various Mn^{III} salen-type complexes that have a potential to exhibit SMM properties. We present here three types of Coulombic aggregations composed of monocationic Mn^{III} salen-type complexes and polyanionic Keggin-type POMs with different charges of 2− and 4−: $[Mn_2(5\text{-MeOsaltmen})_2(acetone)_2][SW_{12}O_{40}]$ (**1**), $[Mn_2(salen)_2(H_2O)_2]_2[SiW_{12}O_{40}]$ (**2**), and $[Mn(5\text{-Brsaltmen})(H_2O)(acetone)]_2[\{Mn_2(5\text{-Brsaltmen})_2\}(SiW_{12}O_{40})]$ (**3**), where 5-Rsaltmen^{2-} = *N*,*N*′-(1,1,2,2-tetramethylethylene)bis(5-R-salicylideneiminate) with R = MeO (methoxy), Br (bromo). These compounds exhibit SMM characters attributed to the Mn^{III} out-of-plane dimeric moieties with an S_T = 4 spin ground state, even though the Mn^{III} dimer precursor compounds were not SMMs. The influence of magnetic correlation between SMMs still remains in **2** competing with the SMM superparamagnetic nature at low ac frequencies, while **1** exhibits typical SMM behavior. Compound **3** has a 1D chain motif with a $[-\{Mn_2\}-(POM)-]^{2-}$ repeating unit, revealing the utility of POMs as a coordinating-donor building unit to form inorganic−organic hybrid functional frameworks.[23] The structures and magnetic properties of **1**−**3** are described.

EXPERIMENTAL SECTION

General Procedures and Materials. All chemicals used during the synthesis were reagent grade. $[Mn_2(5\text{-MeOsaltmen})_2(H_2O)_2](PF_6)_2$ was synthesized by a method similar to that given in ref 24, and $[Mn_2(salen)_2(H_2O)_2](ClO_4)_2$[16] and $[Mn_2(5\text{-Brsaltmen})_2(H_2O)_2](PF_6)_2$[6] were prepared according to the literature methods. $(NBu_4)_2[SW_{12}O_{40}]$ and $(NBu_4)_4[SiW_{12}O_{40}]$ were prepared according to the literature methods in refs 25 and 26, respectively. All procedures were carried out under aerobic conditions at room temperature. *Caution! Perchlorate salts are potentially explosive and should only be handled in small quantities.*

Synthesis of $[Mn_2(5\text{-MeOsaltmen})_2(acetone)_2][SW_{12}O_{40}]$ (1). A solution of $(n\text{-}Bu_4N)_2[SW_{12}O_{40}]$ (1.4 g, 0.405 mmol) in acetone (120 cm^3) was separated into 60 portions, and each portion (2 cm^3) was placed in a narrow diameter glass tube (8 mm in diameter) to form a bottom layer. A solution of $[Mn_2(5\text{-MeOsaltmen})_2(H_2O)_2](PF_6)_2$ (486 mg, 0.405 mmol) in acetone (120 cm^3) separated in 60 portions as well was carefully added on each batch as a top layer. The glass tubes were left undisturbed for 1 week or more to collect greenish brown crystals from all the batches. Yield (based on Mn): 1.10 g, 70.2%. Anal. Calcd for **1**·2(acetone), $SW_{12}O_{52}Mn_2N_4C_{56}H_{76}$; C, 16.89; H, 1.92; N, 1.41. Found: C, 16.99; H, 2.01; N, 159. FT-IR (KBr pellet, 4000−400 cm^{-1}): ν(Schiff base C═N), 1606.4; ν(S−O), 1168.7; ν(W═O_t), 1000.9; ν(W−O_b−W), 897.7, 821.5.

Synthesis of $[Mn_2(salen)_2(H_2O)_2]_2[SiW_{12}O_{40}]$ (2). A solution of $(n\text{-}Bu_4N)_4[SiW_{12}O_{40}]$ (1.53 g, 0.405 mmol) in nitromethane (120 cm^3) was separated into 60 portions with 2 cm^3 for each batch and placed into narrow diameter glass tubes (8 mm in diameter), respectively (bottom layer). After this time, a mixed solvent of nitromethane and acetone (1/1 v/v, 1 cm^3) was added onto the bottom layer as a middle layer as a means to slow the rate of diffusion. Finally, a solution of $[Mn_2(salen)_2(H_2O)_2](ClO_4)_2$ (360 mg, 0.41 mmol) in acetone (120 cm^3) separated in 60 portions as well was carefully added on the middle layer of each batch as a top layer. The glass tubes were left undisturbed for 1 week or more to collect brown crystals. Yield (based on Mn): 529.0 mg, 57.4%. Anal. Calcd for **2**·8H_2O·3(acetone), $C_{73}H_{98}Mn_4N_8O_{63}SiW_{12}$: C, 19.27; H, 2.17; N, 2.46. Found: C, 19.51; H, 1.95; N, 2.81. FT-IR (KBr pellet, 4000−400 cm^{-1}): ν(Schiff base C═N), 1598.7; ν(Si−O), 1047.2; ν(W═O_t), 972.0; ν(W−O_b−W), 919.9, 796.5.

Synthesis of $[Mn(5\text{-Brsaltmen})(H_2O)(acetone)]_2[\{Mn_2(5\text{-Brsaltmen})_2\}(SiW_{12}O_{40})]$ (3). A solution of $(n\text{-}Bu_4N)_4[SiW_{12}O_{40}]$ (459 mg, 0.123 mmol) in nitromethane (36 cm^3) was separated into 18 portions with 2 cm^3 for a batch and placed into narrow diameter glass tubes (8 mm in diameter), respectively, to make a bottom layer. After this time, a mixed solvent of nitromethane and acetone (1/1 v/v, 1 cm^3), as a middle layer, was added onto the bottom layer as a means to slow the rate of diffusion. Finally, a solution of $[Mn_2(5\text{-Brsaltmen})_2(H_2O)_2](PF_6)_2$ (162 mg, 0.12 mmol) in acetone (36 cm^3) separated in 18 portions as well was carefully added on the middle layer of each batch as a top layer. The glass tubes were left undisturbed for 1 week or more to collect brown crystals. Yield (based on Mn): 74.4 mg, 21.5%. Anal. Calcd for **3**·3(CH_3NO_2)·2(acetone), $C_{75}H_{143}Mn_4N_{11}O_{73}SiW_{12}Br_8$: C, 20.02; H, 2.53; N, 2.70. Found: C, 20.21; H, 2.13; N, 2.99. FT-IR (KBr pellet, 4000−400 cm^{-1}): ν(Schiff base C═N), 1600.6; ν(Si−O), 1079.0; ν(W═O_t), 972.0; ν(W−O_b−W), 919.9, 797.4.

Physical Measurements. Infrared spectra were measured using a KBr disk with a HORIBA FT-720 spectrophotometer. Thermogravimetric analysis (TGA) was performed using a Shimadzu DTG-60H instrument in the temperature range from room temperature to 400 °C with a sweep rate of 5 °C/min under N_2 flow. Powder reflection spectra of **1**−**3** were conducted using a Shimadzu UV-3150 spectrophotometer with an attachment for powder reflection spectrometry on $BaSO_4$ pellets. Magnetic susceptibility measurements were conducted using a Quantum Design SQUID magnetometer (MPMS-XL). dc measurements were conducted over the temperature range 1.8−300 K and from −7 to 7 T. ac measurements were performed at frequencies ranging from 1 to 1488 Hz with an ac field amplitude of 3 Oe and in the absence of dc field. The measurements were performed on finely ground polycrystalline samples restrained by Nujol. Diamagnetic contributions were corrected for the sample holder, for Nujol, and for the sample using Pascal constants.[27]

X-ray Crystallography. Single crystals of all compounds were prepared according to the method described in the synthetic procedure. Single crystals having dimensions of 0.13 × 0.29 × 0.12 mm^3 for **1**, 0.19 × 0.26 × 0.12 mm^3 for **2**, and 0.16 × 0.05 × 0.05 mm^3 for **3** were mounted on a thin Kapton film with Nujol and were cooled to 123 ± 1 K by a stream of cooled N_2 gas. Data collections were carried out on a Rigaku CCD diffractometer (Mercury70) with graphite-monochromated Mo Kα radiation (λ = 0.710 70 Å). The full-matrix least-squares refinement on F^2 was performed on the basis of observed reflections and variable parameters, and the refinement cycle was estimated from unweighted and weighted agreement factors of R1 = $\sum||F_o| - |F_c||/\sum|F_o|$ ($I > 2.00\sigma(I)$ and all data) and wR2 = $[\sum(w(F_o^2 - F_c^2)^2)/\sum w(F_o^2)^2]^{1/2}$ (all data). A Sheldrick weighting scheme was used. Neutral atom scattering factors were taken from Cromer and Waber.[28] Anomalous dispersion effects were included in F_c;[29] the values of $\Delta f'$ and $\Delta f''$ were those of Creagh and McAuley.[30] The values for the mass attenuation coefficients are those of Creagh and Hubbell.[31] All calculations were performed using the CrystalStructure crystallographic software package,[32] except for refinement, which was performed using SHELXL-97.[33] It should be noted here that unsuccessful refinements excluded the possibility of the centric space group $P\bar{1}$ (No. 2) for **2** and **3**. Crystallographic data for **1**·2(acetone): formula $C_{56}H_{76}Mn_2N_4O_{52}SW_{12}$, M_r = 3985.35, monoclinic, $P2_1/n$ (No. 14), a = 11.2210(13) Å, b = 17.403(2) Å, c = 21.967(3) Å, β = 97.609(3)°, V = 4251.8(8) Å^3, T = 123(1) K, Z = 2, D_{calc} = 3.113 g cm^{-3}, F_{000} = 3620.00, λ = 0.710 70 Å, μ(Mo Kα) = 165.875 cm^{-1}, 46 700 measured reflections, 9633 unique reflections (R_{int} = 0.0718), R1 = 0.0338 ($I > 2\sigma(I)$), R1 = 0.0389 (all data), and wR2 = 0.0727 (all data) with GOF = 1.055. Crystallographic data for **2**: formula $C_{64}H_{64}Mn_4N_8O_{52}SiW_{12}$, M_r = 4231.27, triclinic, $P1$ (No. 1), a = 13.1100(11) Å, b = 15.9661(12) Å, c = 16.1721(10) Å, α = 73.882(4)°, β = 81.157(6)°, γ = 89.561(6)°, V = 3211.2(5) Å^3, T = 123(1) K, Z = 1, D_{calc} = 2.188 g cm^{-3}, F_{000} = 1922.00, λ = 0.710 70 Å, μ(Mo Kα) =

dx.doi.org/10.1021/ic300215q | Inorg. Chem. 2012, 51, 4824−4832

Table 1. Relevant Bond Distances and Angles of the Bis-μ-Phenoxy Core of Mn^{III} Dimeric Units[a]

compd	indep dimer	Mn−O_a/Å	Mn−O_{in}/Å	Mn−O_{out}/Å	Mn···Mn*/Å	Mn−O_{in}−Mn*/deg	O_{in}−Mn−O_{out}/deg	(J/k_B)/K for Mn^{III} dimer units
1		2.301(5)	1.893(4)	2.335(1)	3.218(1)	98.55(16)	81.45(13)	1.334(6)
2	A	2.24(2)	1.89(2)	2.39(2)	3.252(4)	96.3(6)	83.8(5)	0.98(1) (av)
		2.66(3)	1.90(2)	2.45(2)		98.0(6)	81.9(5)	
	B	2.21(2)	1.90(2)	2.40(2)	3.281(5)	98.3(5)	82.2(6)	
		2.21(2)	1.92(2)	2.42(2)		98.4(5)	81.2(5)	
3		2.204(18)	1.90(3)	2.671(19)	3.507(7)	100.0(10)	79.3(9)	
		2.247(5)	1.87(3)	2.64(2)		99.7(10)	80.8(9)	

[a]Legend: O_a, apical oxygen; O_{in}, in-plane oxygen; O_{out}, out-of-plane oxygen.

111.676 cm^{-1}, 35 158 measured reflections, 22 572 unique reflections (R_{int} = 0.0497), R1 = 0.0487 ($I > 2\sigma(I)$), R1 = 0.0527 (all data), and wR2 = 0.1092 (all data) with GOF = 0.987 and Flack parameter 0.230(11) after treatment by the PLATON SQUEEZE program.[34] Crystallographic data for **3**·CH_3NO_2·2(acetone)·$3H_2O$: formula $C_{93}H_{80}Br_8Mn_4N_9O_{59}SiW_{12}$, M_r = 5360.95, triclinic, $P\bar{1}$ (No. 1), a = 13.782(4) Å, b = 15.611(5) Å, c = 17.204(5) Å, α = 77.258(13)°, β = 71.271(12)°, γ = 70.782(12)°, V = 3283(2) $Å^3$, T = 123(1) K, Z = 1, D_{calc} = 2.712 g cm^{-3}, F_{000} = 2455.00, λ = 0.710 70 Å, μ(Mo Kα) = 133.865 cm^{-1}, 36 383 measured reflections, 23 244 unique reflections (R_{int} = 0.0582), R1 = 0.0706 ($I > 2\sigma(I)$), R1 = 0.0907 (all data), and wR2 = 0.1836 (all data) with GOF = 1.078 and Flack parameter 0.000(1).

The CIF data have been deposited at the Cambridge Data Centre as supplementary publication nos. CCDC-864354, 864355, and 864356 for **1**−**3**, respectively. Copies of the data can be obtained free of charge on application to the CCDC, 12 Union Road, Cambridge CB2 1EZ, U.K. (fax, (+44) 1223-336-033; e-mail, deposit@ccdc.cam.ac.uk).

RESULTS AND DISCUSSION

Syntheses. In this work, the n-Bu_4N^+ salts of two types of tungsten POMs, $[SW_{12}O_{40}]^{2-}$ [25] and $[SiW_{12}O_{40}]^{4-}$,[26] were chosen. These POMs have basically the same core structure called "α-Keggin-type", with the only difference at the central tetrahedral atom S or Si, consequently providing different net charges of 2− and 4−, respectively. The reaction of (n-Bu_4N)$_2$[$SW_{12}O_{40}$] with [Mn^{III}(5-MeOsaltmen)(H_2O)]PF_6 in acetone in a 1:2 molar ratio led to the formation of counterion-substituted aggregation with Mn:POM = 2:1: [Mn_2(5-MeOsaltmen)$_2$(acetone)$_2$][$SW_{12}O_{40}$] (**1**). Similarly, the reaction of (n-Bu_4N)$_4$[$SiW_{12}O_{40}$] with [Mn^{III}(salen)(H_2O)]ClO_4 in nitromethane/acetone in a 1:2 molar ratio also gave a similar aggregation, but with Mn:POM = 4:1: [Mn_2(salen)$_2$-(H_2O)$_2$]$_2$[$SiW_{12}O_{40}$] (**2**). Independent of the kind of salen-type ligand used, the reactions between Mn^{III} salen-type complexes and Keggin-type POMs thus tend to yield all-counterion-substituted Coulombic sets of Mn/POM. Indeed, the use of [Mn^{III}(5-Brsaltmen)(H_2O)]PF_6 instead of [Mn^{III}(salen)(H_2O)]ClO_4 for the last reaction gave an aggregation with an identical Mn:POM ratio of 4:1: [Mn(5-Brsaltmen)(H_2O)(acetone)]$_2$[{Mn_2(5-Brsaltmen)$_2$}-($SiW_{12}O_{40}$)] (**3**). Nevertheless, the structures and crystal packings are strongly dependent on the structure of precursor complexes, solvents used, and coordination affinity if the precursor complexes are candidates for coordinating building blocks as the units used in this work. Therefore, while **1** and **2** are aggregations of discrete dicationic Mn^{III} salen-type out-of-plane dimers (abbreviated henceforth as [Mn_2]) and anionic POMs, **3** contains a one-dimensional (1D) assembly comprised of a $[-\{Mn_2\}-POM-]^{2n-}$ repeating unit, with two discrete Mn monomers axially capped by water and acetone molecules (vide infra). Note that the reaction of [Mn^{III}(5-MeOsaltmen)-(H_2O)]PF_6 with (n-Bu_4N)$_4$[$SiW_{12}O_{40}$] also yields an aggregation with Mn:POM = 4:1, but it cocrystallizes as two types of materials: as a 1D chain material like **3** and as a discrete material like **2**, including the out-of-plane dimer of [Mn_2(5-MeOsaltmen)$_2$(acetone)$_2$]$^{2+}$ and the hydrogen-bonded dimer of [Mn(5-MeOsaltmen)(H_2O)(acetone)]$^+$.[35]

Structures. Compounds **1** and **2** are regarded as simple Coulombic aggregations of discrete ionic units. Compound **1** crystallizes in the monoclinic space group $P2_1/n$ (No. 14) and contains one [Mn_2] dimeric unit, [Mn_2(5-MeOsaltmen)$_2$-(acetone)$_2$]$^{2+}$, and one POM unit, $[SW_{12}O_{40}]^{2-}$, in the formula unit, where both units have inversion centers at the midpoint of Mn···Mn vector and at the S atom, respectively (Z = 2). The [Mn_2] unit has a typical dimeric feature paired by an out-of-plane self-dimerization, where acetone molecules occupy the apical sites of out-of-plane positions. Thus, the Mn^{III} ion takes an elongated octahedral geometry with a Jahn−Teller distortion along the out-of-plane axis. The relevant bond distances and angles of the bis-μ-phenoxy core, together with those for **2** and **3**, are summarized in Table 1. It should be mentioned that the structure of the bridging core is closely associated with the magnetic exchange between Mn ions;[24] this point will be discussed for all compounds in the sections discussing magnetism (vide infra). The $[SW_{12}O_{40}]^{2-}$ anion maintains a polygon of α-Keggin type with a tetrahedral central SO_4 unit. Since the inversion center is located at the central S atom, the SO_4 group is disordered to be a cubic geometry as SO_8 with an atomic occupancy of 0.5 for O atoms.

By presenting bulky POM units as counteranions, the [Mn_2] dimeric units are well separated in the bc plane but are adjacent along the a axis, forming segregated columns (Figure 1). The nearest intermolecular Mn···Mn distance is thus found along the a axis with 9.743(2) Å.

Compound **2** crystallizes in the triclinic space group $P\bar{1}$ (No. 1) and contains two [Mn_2] dimeric units, [Mn_2(salen)$_2$-(H_2O)$_2$]$^{2+}$, and one POM unit, $[SiW_{12}O_{40}]^{4-}$, where the two [Mn_2] units (A and B; see Figure 2) are structurally independent under the acentric space group, albeit much smaller in their differences. The two [Mn_2] units take a typical out-of-plane dimeric motif with water molecules at apical positions. The details of bond distances and angles of the bridging core structures of Mn^{III} dimers are given in Table 1. Although the error deviation seems to be a little large, the structure of Mn^{III} dimers is basically quite similar to that of [Mn_2(salen)$_2$(H_2O)$_2$](ClO_4)$_2$ with Mn−O_{out} = 2.412(6) Å (O_{out} = out-of-plane bridging oxygen).[16] The $[SiW_{12}O_{40}]^{4-}$ anion has the α-Keggin-type structure, in which the central Si atom has a tetrahedral geometry as well as the S atom of $[SW_{12}O_{40}]^{2-}$ in **1**.

The [Mn_2] units and POM units form segregated columns along the a axis as in **1**, and the respective columns are alternately arranged along the b and c axes (Figure 2).

dx.doi.org/10.1021/ic300215q | Inorg. Chem. 2012, 51, 4824−4832

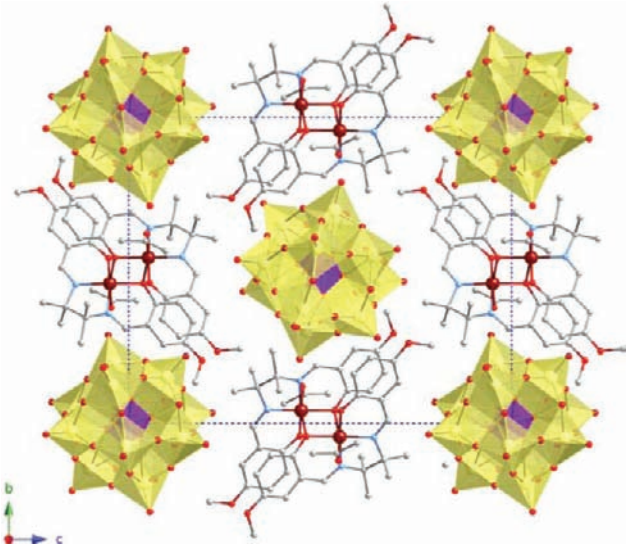

Figure 1. Packing drawing of **1** projected along the *a* axis: C, gray; N, pale blue; O, red; Mn, wine red; S, purple; Mo, yellow. Hydrogen atoms and crystallization solvents are omitted for clarity.

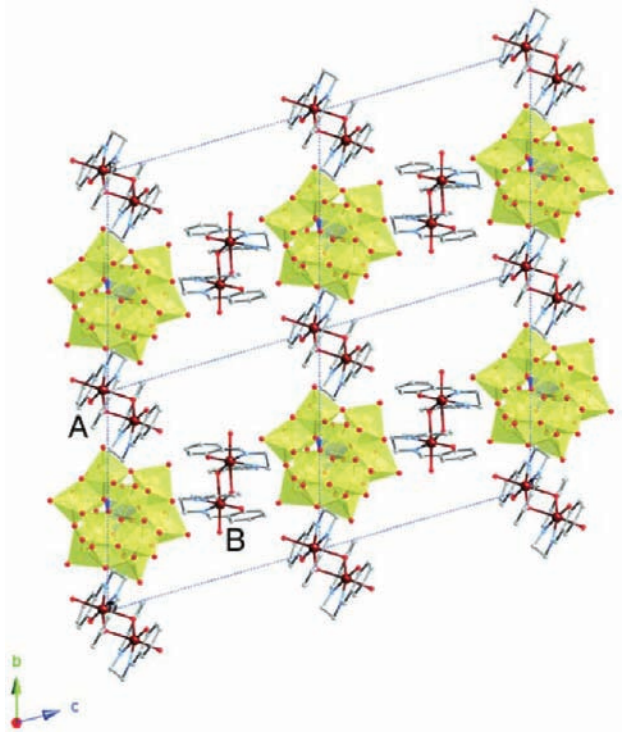

Figure 2. Packing drawing of **2** projected along the *a* axis, where the crystallographically independent out-of-plane dimers A and B were located with adjacent POMs along the *b* and *c* axes, respectively: C, gray; N, pale blue; O, red; Mn, wine red; Si, blue; Mo, yellow. Hydrogen atoms and crystallization solvents are omitted for clarity.

However, the dimers A and B in the unit are adjacent to each other; thus, the nearest interdimer Mn···Mn distance is found between A and B units in the *bc* plane at 7.565(4) Å, significantly shorter than the distance in **1**.

Compound **3** crystallizes in the triclinic space group *P*1 (No. 1) (see the Experimental Section). This compound contains four $[Mn^{III}(5\text{-Brsaltmen})]^{+}$ moieties with one $[SiW_{12}O_{40}]^{4-}$ unit that takes an α-Keggin core; two of them exist as monomers capped by water and acetone molecules at the axial positions, $[Mn^{III}(5\text{-Brsaltmen})(H_2O)(\text{acetone})]^{+}$, and the other two moieties form an out-of-plane dimer, $[Mn^{III}_2(5\text{-Brsaltmen})_2]^{2+}$ (Figure 3a). This Mn^{III} dimer moiety connects the $[SiW_{12}O_{40}]^{4-}$ unit through terminal oxo groups that are just positioned at opposite sides of the Keggin core with Mn(1)–O(9) = 2.204(18) Å, Mn(2)–O(21)* = 2.247(5) Å, W(2)–O(9)–Mn(1) = 156.1(13)°, and W(8)–O(21)–Mn(2)** = 151.0(11)°, forming a linear 1D chain with a repeating unit of $[-\{Mn_2\}-POM-]^{2-}$ (Figure 3b). It should be mentioned that

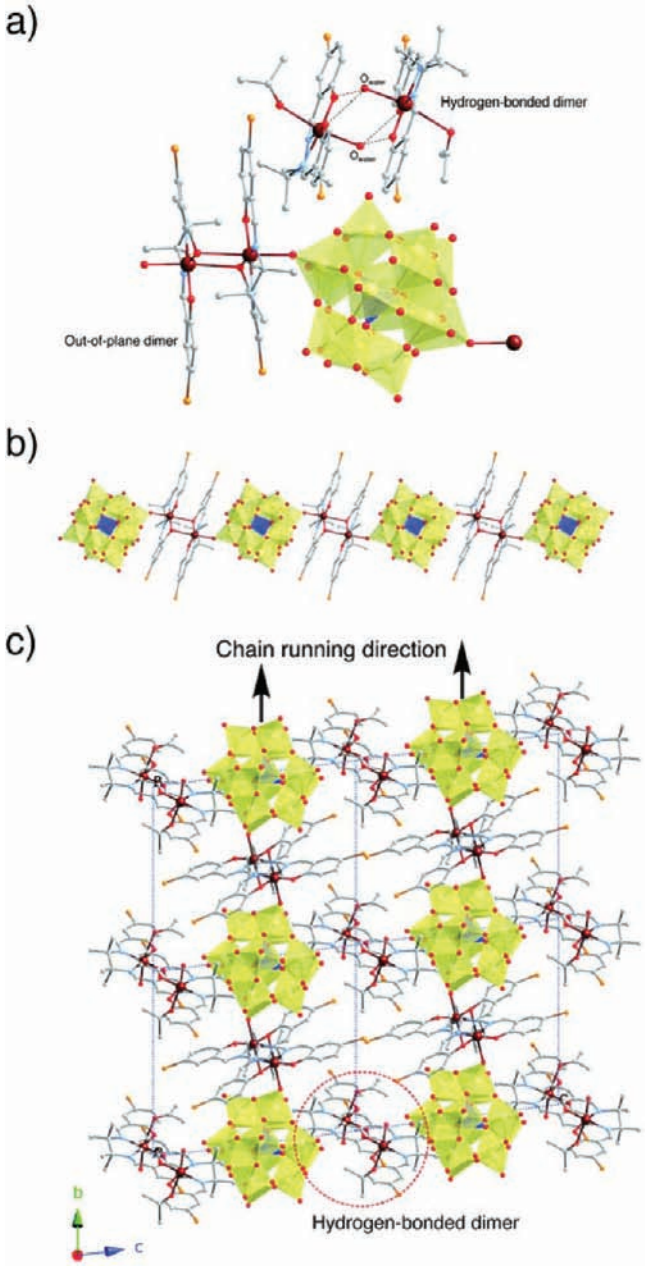

Figure 3. Structure of the formula unit of **3** (a), the chain motif composed of out-of-plane dimers $[Mn^{III}_2(5\text{-Brsaltmen})_2]^{2+}$ and $[SiW_{12}O_{40}]^{4-}$ (b), and a packing drawing projected along the *a* axis, where the chains are running along the *b* axis and the hydrogen-bonded dimers (red dotted circle) are adjacently located between POMs along the *c* axis (c): C, gray; N, pale blue; O, red; Br, orange; Mn, wine red; Si, blue; Mo, yellow. Hydrogen atoms and crystallization solvents are omitted for clarity.

dx.doi.org/10.1021/ic300215q | *Inorg. Chem.* 2012, 51, 4824–4832

low-dimensional coordination polymers based on POMs, as the 1D chain complex in **3**, are indeed not frequent: in particular, in cases using "hard" transition-metal ions. The relevant bond distances and angles of the Mn^{III} dimeric core are given in Table 1. The two monomers also show a Jahn−Teller distortion around the Mn^{III} ion, where the elongated axis is arranged along the out-of-plane direction of the ligand where the water and acetone molecules are occupied. It is noteworthy that these two monomers form a self-assembled supramolecular dimer connected to each other by making hydrogen bonds between H_2O at the apical site and phenoxy oxygen atoms of the 5-Brsaltmen ligand with an average $O_{water}\cdots O_{Ph}$ distance of 2.95 Å (Figure 3a).[10]

The chains run along the (1−10) direction on the *ab* plane, making a segregated layer stacked along the *c* axis with the nearest intrachain (through POM) and interchain Mn···Mn distances of 14.606(7) and 11.317(8) Å, respectively (Figure 3c). Thus, Mn^{III} dimers are well separated by POM units, and this assures weak interactions between the dimers along the chain axis. The nearest intermolecular Mn···Mn distance is found between the hydrogen-bonded dimer and the out-of-plane dimer of the chain at a distance of 7.834(7) Å ($=Mn(2)_{dimer}\cdots Mn(3)_{monomer}$), where the hydrogen-bonded dimers (two monomers) are located between chain layers (Figure 3c).

dc Magnetization Measurements. Compounds **1** and **2** contain dimers of $[Mn^{III}_2(SB)_2(Solv)_2]^{2+}$ (SB = salen-type ligands; Solv = solvent molecules) with anionic POMs of $[SW_{12}O_{40}]^{2-}$ and $[SiW_{12}O_{40}]^{4-}$, respectively. Since the POM moieties are expected to be diamagnetic, the magnetic properties of **1** and **2** should originate from the Mn^{III} dimers. Figure 4 shows the temperature dependence of the χT values of

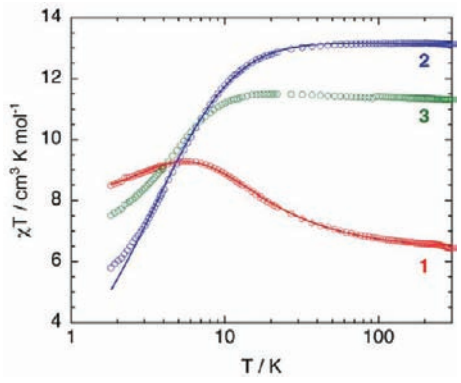

Figure 4. Temperature dependence of χT values of **1** (red), **2** (blue), and **3** (green), where the solid lines for **1** and **2** represent the best-fit lines simulated by using a dimer model of $S = 2$ taking account of magnetic anisotropy and interdimer interactions (see text).

1 and **2**. Reflecting the formula ratio of two Mn dimers in **2** in comparison to one Mn dimer in **1**, the χT value of **2** at 300 K is almost twice of that of **1**, but the entire features of $\chi T-T$ plots are much different for **1** and **2**. For **1**, the χT value of 6.45 cm^3 K mol^{-1} at 300 K continuously increases with decreasing temperature, reaching the maximum value 9.28 cm^3 K mol^{-1} at 5.6 K, and then decreases to 8.48 cm^3 K mol^{-1} at 1.8 K. This behavior is rather typical for Mn^{III} out-of-plane dimers that exhibit SMM properties, and the increase of χT with decreasing temperature is due to ferromagnetic exchange interactions between Mn^{III} ions via a biphenolate bridge to derive an $S_T = 4$ spin ground state. To estimate the exchange coupling, the χT value was simulated using a Heisenberg dimer model of $S = 2$ with a spin Hamiltonian, $H = -2JS\cdot S + D_{Mn}S_z^2 - 2zJ'\langle S\rangle$, where D_{Mn} is the zero-field splitting parameter for a single Mn ion and J' is the interdimer interactions considered in the frame of the mean-field approximation with the z value that represents the number of neighboring dimers. The obtained adequate parameter set is $g = 2.066(1)$, $J/k_B = 1.334(6)$ K, $D_{Mn}/k_B = -4.17(4)$ K, and $zJ'/k_B = 0.016(1)$ K (red line in Figure 4). The negative D_{Mn} value and positive J value are in good agreement with those found in related Mn^{III} salen-type dimers and SMMs.[1,3−5,15,16,24] From the small value of zJ' (positive but $zJ' \approx 0$),[36] we realize that interdimer interactions are negligibly weak, and this should result from significantly longer interdimer distances over 9 Å. The field dependence of the magnetization ($M-H$ curve) of **1** shows a typical behavior of anisotropic paramagnetic state without any hysteresis coercivity and inflection that may suggest the presence of long-range order (Figure S1, Supporting Information).

Meanwhile, for **2**, the χT value, 13.13 cm^3 K mol^{-1} at 300 K, is almost constant down to 50 K and then decreases gradually to reach 5.75 cm^3 K mol^{-1} at 1.8 K (Figure 4). This feature is seemingly due to the domination of antiferromagnetic coupling between Mn^{III} ions in the dimer. However, considering the generality of ferromagnetic contribution in the Mn^{III} out-of-plane dimer (vide infra), the monotonically decreasing feature of χT in **2** is the result of two competing interactions where interdimer antiferromagnetic contributions overwhelm the intradimer ferromagnetic interaction. By simulating the $\chi T-T$ plot of **2** using the dimer model used for **1** (blue line in Figure 4), the following parameter set was obtained, $g = 2.091(1)$, $J/k_B = 0.98(1)$ K, $D_{Mn}/k_B = -4.8(3)$ K, and $zJ'/k_B = -0.856(4)$ K, where all parameters are averaged values for the dimers A and B. The D_{Mn} value is consistent with that for general Mn^{III} salen-type Schiff-base complexes,[3,5,15,24] and the entire feature could be well simulated using positive J and negative J' values with similar degrees of magnitude of J and zJ';[37] this fact is supported by the field dependence of the magnetization curve (Figure S2, Supporting Information) and ac magnetic data (Figures 8 and 9) that prove the SMM behavior of **2** (vide infra). The $M-H$ curve of **2** differs from that of **1**, which has an inflection point (H_{ex}) at 2.52 T (Figure S2), indicating the presence of relatively strong interdimer antiferromagnetic interactions. To estimate the interdimer interactions (zJ') from the inflection behavior, the relation $2|zJ'|S^2 \approx gS\mu_B H_{ex}$ was used, and a relatively large value of $|zJ'| = 0.42$ K with $g = 2.0$ was obtained.[4,38] This value is approximately half of the value estimated from the $\chi T-T$ simulation, which certainly means that interdimer antiferromagnetic interactions are sufficiently large to affect the magnetic behavior of **2**. The competing interdimer antiferromagnetic interaction is caused by a relatively short interdimer distance, Mn···Mn ≈ 7.6 Å, while **1** has a longer distance, Mn···Mn ≈ 9.7 Å (indeed, **1** shows no inflection point in the $M-H$ curve; see Figure S1).

The temperature dependence of χT for **3** is also depicted in Figure 4 as green points. The χT value at 300 K, 11.33 cm^3 K mol^{-1}, which is close to 4 times the spin-only value for $S = 2$ (12.00 cm^3 K mol^{-1} with $g = 2.0$), slightly increases with lowering temperature to reach a maximum of 11.50 cm^3 K mol^{-1} at 18 K and then decreases to 7.51 cm^3 K mol^{-1} at 1.8 K. The increase of χT, albeit small, indicates the ferromagnetic interaction in the out-of-plane dimer that is dominating at high temperatures. However, the small changes of the χT plot

dx.doi.org/10.1021/ic300215q | Inorg. Chem. 2012, 51, 4824−4832

suggest that the antiferromagnetic contribution is also crucial in drawing this feature. In fact, the $M-H$ curve has an inflection at ca. 2.75 T (Figure S3, Supporting Information), similar to the case of **2** that reflects the effect of intermolecular antiferromagnetic interactions. Nevertheless, **3** contains two types of dimers; therefore, it is not easy to evaluate the magnetic behavior of **3** separating the contribution of respective dimers and their mutual relation through interdimer interactions. In general, the out-of-plane coordinating dimer shows a ferromagnetic coupling between spins (vide infra), whereas the hydrogen-bonded dimer may provide an opposite contribution: namely, an antiferromagnetic coupling through hydrogen bonds, as seen in the similar supramolecular hydrogen-bonded dimer $[Mn(5\text{-TMAMsalen})(H_2O)_2]_2$ (5-TMAMsalen = 5-trimethylammoniomethylsalicylideneiminate; $J' = -0.50(5)$ K).[10] In addition, the interdimer interaction may be measurable only when the *interdimer* distance is relatively small, such as ~7 Å for **2**. These two antiferromagnetic contributions should be associated with the inflection of the $M-H$ curve. However, the main contribution in **3** is provided by the hydrogen-bonded dimers (see ac Magnetization Measurements).

We should comment about the correlation between the exchange coupling J and the bis-μ-phenoxo structure. The family of Mn^{III} salen-type out-of-plane dimers generally shows ferromagnetic couplings owing to the accidental orthogonality directly associated with the bridging angle of $Mn-O_{Ph}-Mn$, and the magnitude of coupling is empirically dependent on the length of $Mn-O_{Ph}$,[24] although it is also strongly affected by substituents of salen-type ligands.[39] As shown in Table 1, the angle of $Mn-O_{Ph}-Mn$, 96–100°, in the present system is typical of values generally found in related dimers, where the d_{z^2} orbital corresponding to the Jahn–Teller axis with an unpaired spin on a Mn ion and the empty $d_{x^2-y^2}$ orbital on another Mn ion are coupled via p orbitals on O_{Ph} following Hund's rule. The dc magnetic measurements revealed that all compounds contain ferromagnetically coupled dimers with a spin ground state of $S_T = 4$, which are very likely candidates for SMM. Even though a magnetic simulation has not been done for **3** to avoid overparameterization, the dimer units of the present family with a short $Mn-O_{Ph}$ distance of 2.3–2.7 Å would be preferred dimers that derive relatively strong ferromagnetic couplings according to the relation of J vs $Mn-O_{Ph}$ distances reported previously.[24]

ac Magnetization Measurements. The relaxation behavior of the magnetization of **1**–**3** has been studied using ac susceptibility measurements at several dc fields and an oscillating 3 Oe ac field as a function of frequency (1–1488 Hz) and temperature (1.8–5 K). The ac susceptibility was at first measured as a function of frequency at 1.8 K under several dc fields (Figures 5, 8, and 10 for **1**–**3**, respectively). For **1** (Figure 5), under $H_{dc} = 0$, no clear peak for the out-of-phase (χ'') signal is observed even at 1.8 K, but it is indicial at high frequencies. When dc fields are applied, a clear peak of χ'' appears and shifts to lower frequencies with increasing dc field; however, the shifts became small at $H_{dc} \geq 500$ Oe, clearly indicating the field dependence of the relaxation time (τ) generally observed in SMMs.[2c] Figure 6 is a plot of τ deduced from the peak frequency ν_{peak}, $\tau = 1/(2\pi\nu_{peak})$, as a function of dc field. The τ value becomes greater with increasing field and is almost constant at fields above 1.5 kOe. This behavior should be characteristic of SMMs and is due to the suppression of quantum tunneling of the magnetization (QTM) by applying

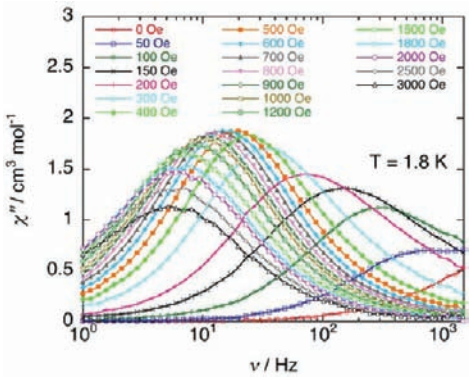

Figure 5. Out-of-phase ac susceptibility (χ'') of **1** at 1.8 K as a function of frequency (ν) under applying several dc fields of 0–3 kOe.

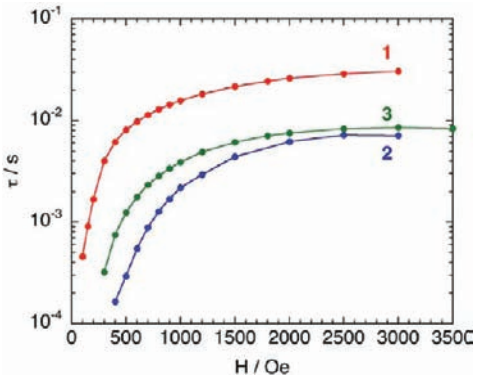

Figure 6. Field dependence of relaxation time (τ) of **1**–**3** at 1.8 K, where τ was estimated from the data in Figures 5, 8, and 10, respectively.

dc fields.[2c,4,5] To compare the effective energy barriers for the relaxation of magnetization (Δ_{eff}), the frequency dependence of ac susceptibility was measured at several temperatures at a fixed dc field of 300, 600, or 1 kOe, and the deduced relaxation times were plotted vs $1/T$ to create Arrhenius plots for the respective fields (Figure S4, Supporting Information). The estimated Δ_{eff} and τ_0 values from the linear Arrhenius plots are $\Delta_{eff}(300\ Oe) = 15.9$ K and $\tau_0(300\ Oe) = 6.1 \times 10^{-7}$ s, $\Delta_{eff}(600\ Oe) = 18.4$ K and $\tau_0(600\ Oe) = 3.7 \times 10^{-7}$ s, and $\Delta_{eff}(1\ kOe) = 19.7$ K and $\tau_0(1\ kOe) = 3.2 \times 10^{-7}$ s. Finally, ac susceptibility was measured as a function of temperature (1.8–5 K) at $H_{dc} = 1.5$ kOe (Figure 7), in which a blocking of in-phase susceptibility (χ') is clearly observed at frequencies above 30 Hz, and these blockings yielded a new Arrhenius plot with $\Delta_{eff}(1.5\ kOe) = 22.8$ K and $\tau_0(1.5\ kOe) = 8.2 \times 10^{-8}$ s (Figure S4). It is noteworthy that the obtained Δ_{eff} values have a trend of $\Delta_{eff}(300\ Oe) < \Delta_{eff}(600\ Oe) < \Delta_{eff}(1\ kOe) < \Delta_{eff}(1.5\ kOe)$ and are in the typical range for Mn^{III} salen-type dimeric SMMs with $S_T = 4$.[3,5] Furthermore, the range of τ_0 (10^{-7}–10^{-8} s) is consistent with that for general SMMs.[2b,c]

The ac susceptibility behavior of **2** is basically similar to that of **1** but is crucially different at low frequencies. As seen in Figure 8, there is a field-independent peak at $\nu \leq 1$ Hz, in addition to the general field dependence of χ'' vs ν similar to that for **1**. This anomaly of χ'' at low frequencies can be also observed in the temperature dependence of ac susceptibility at zero dc field (Figure 9a); the anomalous variation of $\chi''-T$ is observed at temperatures below 2.5 K. Such a peak independence of field could be observed in network systems

dx.doi.org/10.1021/ic300215q | Inorg. Chem. 2012, 51, 4824–4832

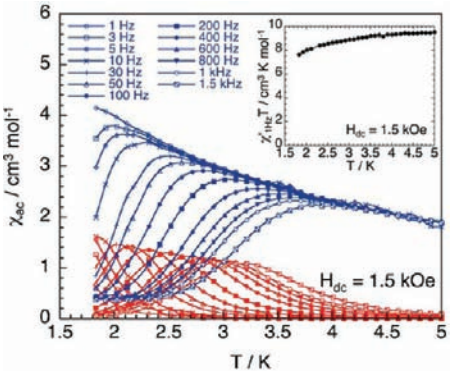

Figure 7. Temperature dependence of ac susceptibilities (χ', blue; χ'', red) of **1** on application of a dc field of 1.5 kOe. Inset: $\chi'_{1\ \mathrm{Hz}}T-T$ plot for the in-phase ac susceptibility at 1 Hz frequency ($\chi'_{1\ \mathrm{Hz}}$).

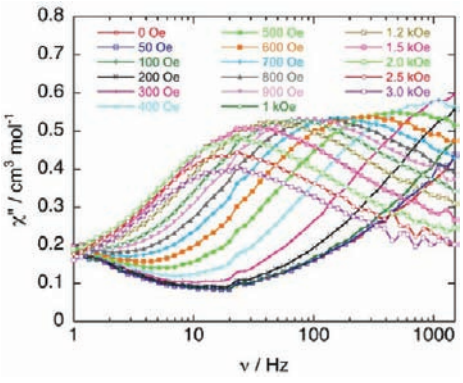

Figure 8. Out-of-phase ac susceptibility (χ'') of **2** at 1.8 K as a function of frequency (ν) on application of several dc fields of 0−3 kOe.

based on SMMs that possibly involve inter-SMM antiferromagnetic ordering.[40−42] It is thus very likely that **2** is a magnetically competing system where SMM character and long-range magnetic ordering are cooperative as a function of ac frequency.[40,43,44] This feature agrees with the characteristics of the structure of **2**, which revealed a short interdimer distance and a relatively large zJ' value evaluated from the simulation of the $\chi T-T$ plot and the inflected $M-H$ curve. As observed at higher frequencies, the χ'' peak is, nevertheless, strongly dependent on dc field, and τ estimated from the peak frequency becomes longer at high fields up to 2.5 kOe (at H_{dc} = 3 kOe, it is constant) (Figure 6). The Arrhenius plots made at H_{dc} = 1 and 1.5 kOe give variable parameters of Δ_{eff} and τ_0: Δ_{eff}(1 kOe) = 15.4 K and τ_0(1 kOe) = 4.1 × 10^{-7} s, Δ_{eff}(1.5 kOe) = 21.2 K and τ_0(1.5 kOe) = 4.4 × 10^{-8} s (Figure S5, Supporting Information), consistent with values for isolated Mn^{III} dimer SMMs.[3,5,15] Indeed, ac susceptibility measured as a function of temperature (1.8−5 K) at H_{dc} = 1.5 kOe reveals the occurrence of blockings of χ' at frequencies above 30 Hz without anomalous peak (Figure 9b). This ac behavior is very similar to that of the 2D networked SMMs that exhibit significant inter-SMM interactions switchable by ac fields.[40a,44]

Even though the dc behavior of **3** is similar to that of **2**, the presence of the inflection in the $M-H$ curve overwhelming any cooperative antiferromagnetic interaction, their ac behavior is rather close to that of **1**; namely, there is no remarkable anomaly originating from inter-SMM long-range correlations in the plot of χ'' vs ν for **3** (Figure 10). This is quite strange, because the inflection field (2.75 T) is significantly higher in

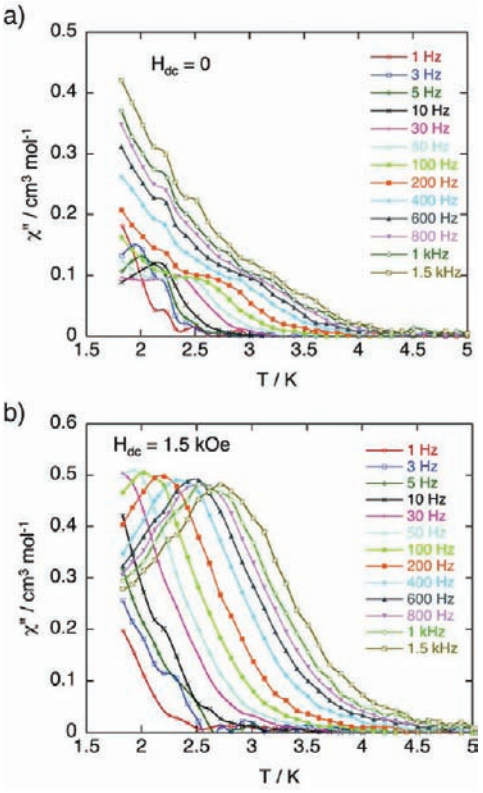

Figure 9. Variable-frequency χ'' values of **2** as a function of temperature measured at 0 (a) and 1.5 kOe (b) dc field.

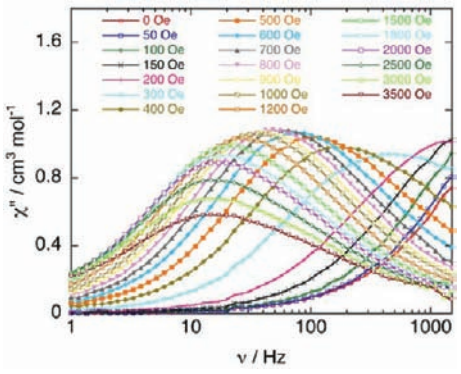

Figure 10. Out-of-phase ac susceptibility (χ'') of **3** at 1.8 K as a function of frequency (ν) on application of several dc fields of 0−3.5 kOe.

comparison to that observed in **2**, and the corresponding antiferromagnetic interactions are very likely to allow the suppression of SMM behavior if such an antiferromagnetic contribution can be attributed to interdimer/intermolecular interactions, as seen in the case of **2**. The fact is, however, that the main contribution of antiferromagnetic interactions causing the inflection of the $M-H$ curve for **3** is probably a result of the hydrogen-bonded dimer (intradimer) rather than the interdimer/intermolecular interactions.[45] Hence, the hydrogen-bonded dimer derives a singlet spin state at significantly lower temperatures; this indicates that the Mn^{III} out-of-plane dimeric unit is magnetically isolated. Indeed, the values of $\chi'T$ for **3** measured at temperatures below 5 K on application of H_{dc} = 1.5 kOe (inset of Figure 11) are very similar to those for **1** (inset of Figure 7), roughly converging the value of χT = 10.0

dx.doi.org/10.1021/ic300215q | Inorg. Chem. 2012, 51, 4824−4832

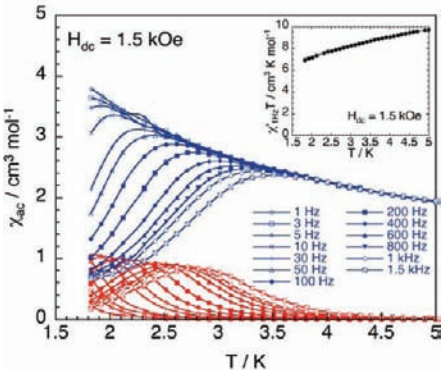

Figure 11. Temperature dependence of ac susceptibilities (χ', blue; χ'', red) of **3** on application of a dc field of 1.5 kOe. Inset: $\chi'_{1\ \mathrm{Hz}}T-T$ plot for the in-phase ac susceptibility at 1 Hz frequency ($\chi'_{1\ \mathrm{Hz}}$).

$cm^3\ K\ mol^{-1}$ with $g = 2$ for an isolated $S_T = 4$ state. As shown in Figure 11, the blocking behavior of χ' can be found at temperatures above 1.8 K on application of ac frequencies above 30 Hz, similar to the case of **1**. The field dependence of τ is plotted in Figure 6, where τ becomes constant at fields above 2.5 kOe. The frequency dependence of ac susceptibility was measured at several temperatures on fixing an applied dc field at 500, 1000, or 1500 Oe to give Arrhenius plots of τ vs $1/T$ at the respective fields (Figure S6, Supporting Information). The obtained Δ_{eff} and τ_0 values are Δ_{eff}(500 Oe) = 14.7 K and τ_0(500 Oe) = 3.8×10^{-7} s, Δ_{eff}(1 kOe) = 17.6 K and τ_0(1 kOe) = 2.4×10^{-7} s, and Δ_{eff}(1.5 kOe) = 21.0 K and τ_0(1.5 kOe) = 6.4×10^{-8} s, consistent with parameters for Mn^{III} dimeric SMMs.

CONCLUSION

The reaction of dicationic Mn^{III} salen-type dimers with di- and tetraanionic α-Keggin-type POMs was performed to examine the effect of Keggin-type anions as magnetic separators in $[Mn_2]^{2+}$ dimers that intrinsically exhibit SMM character, and three types of Coulombic aggregations containing $[Mn_2]^{2+}$ were synthesized. Independent of the formula ratio, Mn^{III} dimers and POM units are arranged to form respective segregated columns along the direction of the unit cell (the *a* axis for the present compounds) and are packed alternately, like a checkerboard or a square-grid network as projected along the *a* axis, to evenly separate identical species in a crystal. The 1D chain in **3** composed of the alternation of SMM and POM units is unique. Such POM-based coordination polymers could be some of the structural models for magnetic/electronic functional molecules.[46] Consequently, an intrinsic property, SMM behavior, of Mn^{III} dimers has been well characterized in this system, even though the interdimer interactions still crucially affect the overall behavior of compounds as seen in the case of **2**. The magnetic behavior of **2** is similar to that of a 2D-networked SMM compound, $[Mn_4(hmp)_4Br_2(OMe)_2(dcn)_2]\cdot 0.5H_2O\cdot 2THF$ (hmp^- = 2-hydroxymethylpyridinate; dcn^- = dicyanamidate), where magnetic correlations among SMM units compete with the Ising nature of the respective SMM units.[40,44]

Most POMs are polyanionic large clusters with a diameter of ~1 nm as Keggin-type clusters; the point as a magnetic separator was the focus in the present work. Also, POMs have characteristic properties such as structural diversity, electronic-structural diversity, high redox activity, and relatively high stability even in several oxidation states. When these characteristics, in particular electron or spin activity, are organically connected to assembled (cluster) units rationally arranged in the solid state, new material systems, such as a unique strongly correlated electronic system, could be developed.

ASSOCIATED CONTENT

Supporting Information

CIF files giving X-ray crystallographic data and figures giving magnetic data that support the discussions. This material is available free of charge via the Internet at http://pubs.acs.org.

AUTHOR INFORMATION

Corresponding Author

*Tel: +81-76-264-5697. Fax: +81-76-264-5742. E-mail: miyasaka@se.kanazawa-u.ac.jp.

Notes

The authors declare no competing financial interest.

ACKNOWLEDGMENTS

This work was partially supported by a Grant-in-Aid for Scientific Research from the Ministry of Education, Culture, Sports, Science, and Technology of Japan (Grant No. 21350032).

REFERENCES

(1) Miyasaka, H.; Saitoh, A.; Abe, S. *Coord. Chem. Rev.* **2007**, *251*, 2622.

(2) (a) Christou, G.; Gatteschi, D.; Hendrickson, D. N.; Sessoli, R. *MRS Bull.* **2000**, *25*, 66. (b) Gatteshi, D.; Sessoli, R. *Angew. Chem., Int. Ed.* **2003**, *42*, 268. (c) Gatteschi, D.; Sessoli, R.; Villain, J. *Molecular Nanomagnets*; Oxford University Press: London, 2006.

(3) (a) Miyasaka, H.; Clérac, R.; Wernsdorfer, W.; Lecren, L.; Bonhomme, C.; Sugiura, K.; Yamashita, M. *Angew. Chem., Int. Ed.* **2004**, *43*, 2801. (b) Lü, Z.; Yuan, M.; Pan, F.; Gao, S.; Zhang, D.; Zhu, D. *Inorg. Chem.* **2006**, *45*, 3538.

(4) (a) Kachi-Terajima, C.; Miyasaka, H.; Sugiura, K.; Clérac, R.; Nojiri, H. *Inorg. Chem.* **2006**, *45*, 4381. (b) Kachi-Terajima, C.; Miyasaka, H.; Saitoh, A.; Shirakawa, N.; Yamashita, M.; Clérac, R. *Inorg. Chem.* **2007**, *46*, 5861.

(5) (a) Hiraga, H.; Miyasaka, H.; Takaishi, S.; Kajiwara, T.; Yamashita, M. *Inorg. Chim. Acta* **2008**, *361*, 3863. (b) Hiraga, H.; Miyasaka, H.; Clérac, R.; Fourmigué, M.; Yamashita, M. *Inorg. Chem.* **2009**, *48*, 2887.

(6) Miyasaka, H.; Nezu, T.; Sugimoto, K.; Sugiura, K.; Yamashita, M.; Clérac, R. *Chem. Eur. J.* **2005**, *11*, 1592.

(7) (a) Choi, H. J.; Sokol, J. J.; Long, J. R. *Inorg. Chem.* **2004**, *43*, 1606. (b) Ferbinteanu, M.; Miyasaka, H.; Wernsdorfer, W.; Nakata, K.; Sugiura, K.; Yamashita, M.; Coulon, C.; Clérac, R. *J. Am. Chem. Soc.* **2005**, *127*, 3090.

(8) Coulon, C.; Miyasaka, H.; Clérac, R. *Struct. Bonding (Berlin)* **2006**, *122*, 163.

(9) (a) Clérac, R.; Miyasaka, H.; Yamashita, M.; Coulon, C. *J. Am. Chem. Soc.* **2002**, *124*, 12837. (b) Miyasaka, H.; Clérac, R.; Mizushima, K.; Sugiura, K.; Yamashita, M.; Wernsdorfer, W.; Coulon, C. *Inorg. Chem.* **2003**, *42*, 8203. (c) Saitoh, A.; Miyasaka, H.; Yamashita, M.; Clérac, R. *J. Mater. Chem.* **2007**, *17*, 2002. (d) Miyasaka, H.; Saitoh, A.; Yamashita, M.; Clérac, R. *Dalton Trans.* **2008**, 2422.

(10) Miyasaka, H.; Madanbashi, T.; Sugimoto, K.; Nakazawa, Y.; Wernsdorfer, W.; Sugiura, K.; Yamashita, M.; Coulon, C.; Clérac, R. *Chem. Eur. J.* **2006**, *12*, 7028.

(11) Miyasaka, H.; Madanbashi, T.; Saitoh, A.; Motokawa, N.; Ishikawa, R.; Yamashita, M.; Bahr, S.; Wernsdorfer, W.; Clérac, R. *Chem. Eur. J.* **2012**, in press.

(12) Miyasaka, H.; Julve, M.; Yamashita, M.; Clérac, R. *Inorg. Chem.* **2009**, *48*, 3420.

(13) (a) Coulon, C.; Clérac, R.; Wernsdorfer, W.; Colin, T.; Miyasaka, H. *Phys. Rev. Lett.* **2009**, *102*, 167204. (b) Miyasaka, H.; Takayama, K.; Saitoh, A.; Furukawa, S.; Yamashita, M.; Clérac, R. *Chem. Eur. J.* **2010**, *16*, 3656.
(14) Forment-Aliaga, A.; Coronado, E.; Feliz, M.; Gaita-Arino, A.; Llusar, R.; Romero, F. M. *Inorg. Chem.* **2003**, *42*, 8019.
(15) Wu, Q.; Li, Y.-G.; Wang, Y.-H.; Clérac, R.; Lu, Y.; Wang, E.-B. *Chem. Commun.* **2009**, 5743.
(16) Shyu, H.-L.; Wei, H.-H.; Wang, Y. *Inorg. Chim. Acta* **1999**, *290*, 8.
(17) Clemente-Juan, J. M.; Coronado, E. *Coord. Chem. Rev.* **1999**, *193*−*195*, 361.
(18) (a) Ritchie, C.; Ferguson, A.; Nojiri, H.; Miras, H. N.; Song, Y.-F.; Long, D.-L.; Burkholder, E.; Murrie, M.; Kögerler, P.; Brechin, E. K.; Cronin, L. *Angew. Chem., Int. Ed.* **2008**, *47*, 5609. (b) Compain, J.-D.; Mialane, P.; Dolbecq, A.; Mbomekallé, I. M.; Marrot, J.; Sécheresse, F.; Riviére, E.; Rogez, G.; Wernsdorfer, W. *Angew. Chem., Int. Ed.* **2009**, *48*, 3077. (c) Giusti, A.; Charron, G.; Mazerat, S.; Compain, J.-D.; Milane, P.; Dolbecq, A.; Riviére, E.; Wernsdorfer, W.; Biboum, R. N.; Keita, B.; Nadjo, L.; Filoramo, A.; Bourgoin, J.-P.; Mallah, T. *Angew. Chem., Int. Ed.* **2009**, *48*, 4949. (d) Ibrahim, M.; Lan, Y.; Bassil, B. S.; Xiang, Y.; Suchopar, A.; Powell, A. K.; Kortz, U. *Angew. Chem., Int. Ed.* **2011**, *50*, 4708.
(19) (a) AlDamen, M. A.; Clemente-Juan, J. M.; Coronado, E.; Martí-Gastaldo, C.; Gaita-Ariño. *J. Am. Chem. Soc.* **2008**, *130*, 8874. (b) AlDamen, M. A.; Cardona-Serra, S.; Clemente-Juan, J. M.; Coronado, E.; Gaita-Ariño, A.; Martí-Gastaldo, C.; Luis, F.; Montero, O. *Inorg. Chem.* **2009**, *48*, 3467.
(20) Pope, M. T. *Heteropoly and Isopoly Oxometalates*; Springer: Berlin, 1983.
(21) (a) Sadakane, M.; Steckhan, E. *Chem. Rev.* **1998**, *98*, 219. (b) Müller, A.; Peters, F.; Pope, M. T.; Gatteschi, D. *Chem. Rev.* **1998**, *98*, 239. (c) Coronado, E.; Gómez-García, C. J. *Chem. Rev.* **1998**, *98*, 273. (d) Long, D.-L.; Burkholder, E.; Cronin, L. *Chem. Soc. Rev.* **2007**, *36*, 105. (e) Long, D.-L.; Tsunashima, R.; Cronin, L. *Angew. Chem., Int. Ed.* **2010**, *49*, 1736. (f) Dolbecq, A.; Dumas, E.; Mayer, C. R.; Mialane, P. *Chem. Rev.* **2010**, *110*, 6009.
(22) Kortz, U. *Eur. J. Inorg. Chem.* **2009**, 5056 and manuscripts in cluster issue: polyoxometalates (2009, Vol. 34).
(23) Sawada, Y.; Yuma, Y.; Wataru, K.; Hayashi, Y.; Miyasaka, H. *Chem. Lett.* **2012**, in press, and references therein..
(24) Miyasaka, H.; Clérac, R.; Ishii, T.; Chang, H.-C.; Kitagawa, S.; Yamashita, M. *Dalton Trans.* **2002**, 1528.
(25) Himeno, S.; Takamoto, M.; Hoshiba, M.; Higuchi, A.; Hashimoto, M. *Bull. Chem. Soc. Jpn.* **2004**, *77*, 519.
(26) Yokoyama, A.; Kojima, T.; Ohkubo, K.; Fukuzumi, S. *Inorg. Chem.* **2010**, *49*, 11190.
(27) Boudreaux, E. A., Mulay, L. N., Eds. *Theory and Applications of Molecular Paramagnetism*; Wiley: New York, 1976.
(28) Cromer, D. T.; Waber, J. T. *International Tables for Crystallography*; Kynoch Press: Birmingham, England, 1974; Vol. *IV*, Table 2.2A.
(29) Ibers, J. A.; Hamilton, W. C. *Acta Crystallogr.* **1964**, *17*, 781.
(30) Creagh, D. C.; McAuley, W. J. *International Tables for Crystallography*; Wilson, A. J. C., Ed.; Kluwer Academic: Boston, MA, 1992; Vol. *C*, Table 4.2.6.8, pp 219−222.
(31) Creagh, D. C.; Hubbell, J. H. *International Tables for Crystallography*; Wilson, A. J. C., Ed.; Kluwer Academic: Boston, MA, 1992; Vol. *C*, Table 4.2.4.3, pp 200−206.
(32) *CrystalStructure 4.0.1: Crystal Structure Analysis Package*; Rigaku Corp., Tokyo 196-8666, Japan, 2000−2010.
(33) SHELX97: Sheldrick, G. M. *Acta Crystallogr.* **2008**, *A64*, 112−122.
(34) Spek, A. L. *J. Appl. Crystallogr.* **2003**, *36*, 7.
(35) The two materials crystallize in different shapes of crystals in a batch, and these crystals can be manually picked up to separate them. However, these materials are not described here to avoid mistaking their essentials.
(36) The obtained positive zJ' value indicates the presence of interdimer ferromagnetic interactions, but there is no firm evidence to explain the fact. The magnitude of zJ' is much smaller, so it may be better to consider $zJ' \approx 0$.
(37) This simulation was carried out in the limit of $D_{Mn} < 0$ and $J > 0$, but the distribution of quantitative contributions of D, J, and zJ' is not strict; rather, the large contribution of zJ' in **2** is proved by the $M-H$ curve.
(38) Richard, L. C. *Magnetochemistry*; Springer-Verlag: Berlin, Heidelberg, 1986.
(39) As our empirically based evaluation, the correlation between J and the Mn−O* distance on Mn^{III} dimeric complexes with 5-MeO or 5-Br substituted saltmen-type ligands, does not follow the relation reported previously in ref 24, which gives respective unique linear correlations. This is an unpublished result.
(40) Miyasaka, H.; Nakata, K.; Lecren, L.; Coulon, C.; Nakazawa, Y.; Fujisaki, T.; Sugiura, K.; Yamashita, M.; Clérac, R. *J. Am. Chem. Soc.* **2006**, *128*, 3770.
(41) (a) Goodwin, J. C.; Sessoli, R.; Gatteschi, D.; Wernsdorfer, W.; Powell, A. K.; Heath, S. L. *Dalton Trans.* **2000**, 1835. (b) Affronte, M.; Lasjanunias, J. C.; Wernsdorfer, W.; Sessoli, R.; Gatteschi, D.; Heath, S. L.; Fort, A.; Rettori, A. *Phys. Rev. B* **2002**, *66*, 064408.
(42) Boskovic, C.; Bircher, R.; Tregenna-Piggott, P. L. W.; Güdel, H. U.; Paulsen, C.; Wernsdorfer, W.; Barra, A.-L.; Khatsko, E.; Neels, A.; Stoeckli-Evans, H. *J. Am. Chem. Soc.* **2003**, *125*, 14046.
(43) (a) Fujisaki, T.; Nakazawa, Y.; Oguni, M.; Nakata, K.; Yamashita, M.; Lecren, L.; Miyasaka, H. *J. Phys. Soc. Jpn.* **2007**, *76*, 104602. (b) Yamashita, S.; Fujisaki, T.; Nakazawa, Y.; Oguni, M.; Nakata, K.; Yamashita, M.; Miyasaka, H. *J. Phys. Soc. Jpn.* **2008**, *77*, 073708.
(44) Mito, M.; Ogawa, M.; Deguchi, H.; Yamashita, M.; Miyasaka, H. *J. Appl. Phys.* **2010**, *107*, 124316.
(45) Assuming the inflection of the $M-H$ curve can only be attributed to an antiferromagnetic interaction in the hydrogen-bonded dimer, its exchange coupling constant (J_H) is roughly deduced as $|J_H| = 0.92$ K from the relation of $2|zJ'|S^2 \approx gS\mu_B H_{ex}$ with $z = 1$ and $g = 2$.
(46) Galán-Mascarós, J. R.; Giménez-Saiz, C.; Triki, S.; Gómez-García, C. J.; Coronado, E.; Ouahab, L. *Angew. Chem., Int. Ed.* **1995**, *34*, 1460.